

NLO Electroweak Corrections to Multi-Boson Processes at a Muon Collider

Pia M. Bredt^{,^{a,1} Wolfgang Kilian,^b Jürgen Reuter^{}^a and Pascal Stienemeier^{}^a}

^a*Deutsches Elektronen-Synchrotron DESY, Notkestr. 85, 22607 Hamburg, Germany*

^b*Department of Physics, University of Siegen, Walter-Flex-Str. 3, 57068 Siegen, Germany*

E-mail: pia.bredt@desy.de, kilian@physik.uni-siegen.de,
juergen.reuter@desy.de, pascal.stienemeier@desy.de

ABSTRACT: We present results on NLO electroweak (EW) corrections to multiple massive boson production processes at a future muon collider. Inclusive cross sections with $\mathcal{O}(\alpha)$ corrections for processes for up to four bosons in the final state as well as differential distributions for HZ production are computed for $\sqrt{s} = 3, 10$ and 14 TeV by using FKS subtraction in the NLO EW automated Monte-Carlo framework WHIZARD+RECOLA. Large logarithmic effects due to collinear ISR and EW virtual correction factors as well as the impacts of an energy cut on hard photons are discussed with an emphasis on the properties of Higgsstrahlung. The potential of a proposed muon collider for studying physics of the EW sector is underlined by the EW corrections significantly affecting observables for processes at high energies and boson multiplicities.

¹Corresponding author.

Contents

1	Introduction	1
2	Setup and NLO framework	3
3	Total cross sections and inclusive results of benchmark processes	4
3.1	Collider energy scans for cross sections of HZ and ZZ production	5
3.2	Total NLO cross sections for multi-boson processes	9
4	Differential distributions for NLO EW corrections	15
5	Conclusions and Outlook	19
A	Validation for massive lepton-initiated process setup	21
B	Derivation of the HZ Sudakov correction factor	21

1 Introduction

Our current understanding of electroweak (EW) physics is governed by the Standard Model (SM). The model predicts a simple symmetry structure at the fundamental level, and it yields the correct low-energy limit of electromagnetic, weak, and strong interactions. Yet, genuine EW and Higgs data can justify this theoretical concept only on a rather superficial level. Energy-frontier experiments, in particular at the Large Hadron Collider (LHC), do not access energy scales in EW interactions beyond about 1 TeV. This is less than one order of magnitude above the inherent mass scale of $v = (\sqrt{2}G_F)^{-1/2} = 246$ GeV. The highest multiplicity of the mutual interactions of massive EW particles (t, W, Z, H) that can be probed is three or, in a few cases, four.

If the SM and its symmetry structure are to be established on a deeper level, or modified by new effects at short distance, there is a clear need for collider experiments which are able to directly probe EW interactions at higher energy and higher multiplicity, and simultaneously with better precision than possible today. There are plans for a next-generation hadron collider [1, 2]. Modern lepton-acceleration technology (ILC [3, 4], CLIC [5, 6]) would also allow us to further extend the energy frontier. Recently, colliders based on storage rings with muons have been proposed as a further option for exploring the multi-TeV range, exploiting new ideas for the cooling of the high-energy, high-intensity muon beams [7–12].

A muon collider would indeed become a valuable tool for pushing the limits of the SM: center-of-mass (c.m.) energies beyond 10 TeV are considered technologically feasible. Proposed benchmark values which we will use in this work, are 3 TeV, 10 TeV, and 14 TeV.

The clean lepton-collider environment in conjunction with dedicated detectors will enable exclusive measurements of final states in both leptonic and hadronic channels.

Muons are elementary particles in the SM, so their collisions offer remarkable options for the search for new particles and interactions at the full machine energy. The physics accessible at a muon collider is very similar to the physics at an e^+e^- collider with the same energy (e.g., CLIC with $\sqrt{s} = 3$ TeV) [12]. Moreover, the larger mass of the muon as compared to the electron, reduces dominant effects that dilute leptonic collisions, namely beamstrahlung as a collective beam-beam interaction, and initial-state radiation (bremsstrahlung) as a reduction of the effective c.m. energy due to photon emission.

A high-energy muon collider will thus open up possibilities of studying a rich set of processes with single and multiple EW gauge and Higgs bosons. In this work, we focus on multi-boson production processes $\mu^+\mu^- \rightarrow V^n H^m$ with $V \in \{W^\pm, Z\}$ and $n + m \leq 4$. These processes allow us to scrutinize the EW gauge and symmetry-breaking sector, study Higgs interactions in detail, and search for new (heavy or light) states which couple to the EW sector.

At leading order in the SM couplings, standard universal Monte-Carlo (MC) programs provide detailed predictions for this class of processes, both within the SM and in perturbative extensions such as the Standard-Model Effective Field Theory (SMEFT). In Ref. [13], we computed multi-boson production cross sections with $n + m \leq 4$ for the CLIC e^+e^- collider with $\sqrt{s} \leq 3$ TeV. The results also apply to a muon collider in the same energy range. A dedicated muon-collider study [14] furthermore covered energies up to 30 TeV. The specific phenomenology of lepton spin-flip interactions which distinguishes muons from electrons, was studied for multi-boson production processes in Refs. [15–18].

In order to establish a potential deviation from the predictions of the SM and to claim a potential discovery of new physics, predictions of the SM (or any other reference model) have to be provided with a precision that is at least as good as the combined statistical and systematic uncertainty of the experimental measurement. Due to the high envisaged integrated luminosities and the immense precision of modern highly-granular particle physics detectors with analyses based on particle flow, leading-order (LO) calculations are almost always insufficient to match the experimental precision on the theory side. To this end, in this paper we complement the previous results by cross-section results and exemplary distributions at next-to-leading order (NLO) in the complete SM.

For asymptotically high energy, NLO corrections to exclusive final states are dominated by Sudakov-type double logarithms. The correction to the inclusive EW-singlet total cross section depends only on the SM running couplings as functions of energy, with a rather moderate energy dependence. However, the multiplicity distribution of the exclusive final states within this total rate exhibits a transition to jet-like EW radiation patterns as soon as the vector-boson masses become negligible in the multi-TeV regime. By unitarity, the appearance of high-multiplicity final states is compensated by an eventual logarithmic reduction ($\log s/m_V^2$) of low-multiplicity final states. This reduction can be exponentiated to leading-logarithmic order by standard techniques. A simple estimate suggests EW-jet dominance and strong Sudakov suppression at the highest muon-collider energies (e.g., 30 TeV). Conversely, at 3 TeV higher-order Sudakov logarithms are still subleading compared to

standard NLO perturbative corrections. In this work, we compute the complete fixed-order NLO corrections to multi-boson production processes for a muon collider in the transition region 3...14 TeV, where both logarithmic and non-logarithmic NLO contributions are important.

After a brief overview in Sec. 2 on our setup and methods used for the NLO EW computations we present results on inclusive cross sections in Sec. 3. Included are cross section scans at NLO EW in \sqrt{s} for HZ and ZZ production and more general results to two, three and four bosons in the final state at 3 TeV, and additionally to two and three bosons at 10 and 14 TeV muon collider, respectively. Moreover, in this section an estimate for the ISR effects on the corresponding processes is given by LO cross section results including leading logarithmic (LL) resummation in α of the initial state. In Sec. 4 differential distributions for the process $\mu^+\mu^- \rightarrow HZ$ at the three proposed muon collider energies with and without cuts on hard photons occurring at NLO in α are discussed.

2 Setup and NLO framework

We compute NLO cross sections and distributions for multi-boson processes using the Monte-Carlo event generator **WHIZARD** [19, 20]. This generator is a multi-purpose program for cross-section and distribution calculation as well as for generating simulated event samples; for a recent application to muon-collider EW and Higgs physics cf. [18]. We recently extended **WHIZARD**'s automated framework to account for the complete perturbative NLO corrections in the full SM. While the new NLO module will be documented in detail in a separate publication [21], we summarize methods and features below.

The EW one-loop virtual contributions are provided by **RECOLA** [22], which can account for the full mass dependence of fermions and bosons. Additionally, for NLO QED cross sections for HZ and ZZ , we have used our interface to the one-loop provider **OpenLoops** [23]. Phase-space construction and subtraction follow the FKS scheme [24, 25] (for NLO QCD in the color-flow formalism [26]), fully automatized for lepton and hadron colliders [21, 27].¹ For an appropriate FKS phase-space construction with massive particles in both initial and final state, we adjust the mapping between the Born and real-radiation phase-space parameterizations according to the on-shell projection proposed in [33, 34]. We have generalized this phase-space construction scheme from its original application to factorized processes with massive resonances [32]. The integration proceeds via numerical phase-space sampling with multi-channel adaption [35]. The time-consuming NLO calculations and simulations are heavily facilitated using **WHIZARD**'s MPI-based parallelization [36].

For the numerical results of this study, we define the electromagnetic coupling α at the hard scale of the process in the G_μ input-parameter scheme, thus resumming a certain class of logarithmically enhanced QED corrections. Regarding massive vector bosons, we impose on-shell renormalization conditions and set particle widths to zero, thus maintaining EW gauge invariance in the interference of s -channel and t -channel contributions. Throughout the calculation, we use nonzero masses for all particles except for photon and

¹Earlier versions of **WHIZARD** used special-tailored NLO-EW amplitudes [28, 29] or a different subtraction scheme for QCD-NLO corrections [30–32].

neutrinos, and the corresponding Yukawa couplings are included. While for light quarks and electrons in loops this is merely a technical detail without phenomenological significance, keeping the muon mass nonzero regulates infrared and collinear divergences associated with initial-state radiation. In fact, QED corrections beyond NLO are parameterically of order $(\alpha/\pi)^2 \log^2(s/m_\mu^2) \sim 0.1\%$ which is sufficiently small in the present context. This allows us to treat the colliding $\mu^+\mu^-$ system perturbatively without the need for higher-order resummation or for introducing leptonic parton distribution functions.

We performed technical sanity checks on the implemented FKS subtraction scheme such as checking soft limits (note that for massive emitters, there are no collinear subtractions) and cross checks comparing the FKS real phase-space parameterization to the underlying Born process $\mu^+\mu^- \rightarrow X$ with the LO parameterization of $\mu^+\mu^- \rightarrow X + \gamma$ with a well-defined photon.

Beyond technical checks, we validated explicit NLO EW cross section results of $e^+e^- \rightarrow HZ$ with MCSANCee [37]. The electrons for these checks are treated as massive which is analogous to the setup for processes with massive initial-state muons. The results and details of these rather technical checks are deferred to the appendix A.

For reference, we list the numerical input parameters. They are used consistently for LO and NLO amplitude calculations and for phase-space construction, where applicable.

$$\begin{aligned}
G_\mu &= 1.166379 \cdot 10^{-5} \text{ GeV}^{-2} \\
m_u &= 0.062 \text{ GeV} & m_d &= 0.083 \text{ GeV} \\
m_c &= 1.67 \text{ GeV} & m_s &= 0.215 \text{ GeV} \\
m_t &= 172.76 \text{ GeV} & m_b &= 4.78 \text{ GeV} \\
M_W &= 80.379 \text{ GeV} & m_e &= 0.0005109989461 \text{ GeV} \\
M_Z &= 91.1876 \text{ GeV} & m_\mu &= 0.1056583745 \text{ GeV} \\
M_H &= 125.1 \text{ GeV} & m_\tau &= 1.77686 \text{ GeV} \quad .
\end{aligned}$$

3 Total cross sections and inclusive results of benchmark processes

For the total cross sections, we restrict ourselves to fully inclusive results: a complete treatment of these processes with identified photons in the final state taking into account a sophisticated future experimental setup like fiducial phase space cuts and selection efficiencies is beyond the scope of this study. We dedicate section 4 to a more detailed investigation of hard-photon reduced observables by considering cut criteria on the radiated photon energy for the differential results.

For the results presented in this section we define the relative NLO EW correction δ_{EW} as

$$\delta_{\text{EW}} = \frac{\sigma_{\text{NLO}}^{\text{incl}}}{\sigma_{\text{LO}}^{\text{incl}}} - 1 \quad (3.1)$$

where $\sigma_{\text{LO}}^{\text{incl}}$ and $\sigma_{\text{NLO}}^{\text{incl}}$ are the total inclusive cross sections at LO and NLO EW, respectively. So, this definition is the usual NLO K factor subtracted by one.

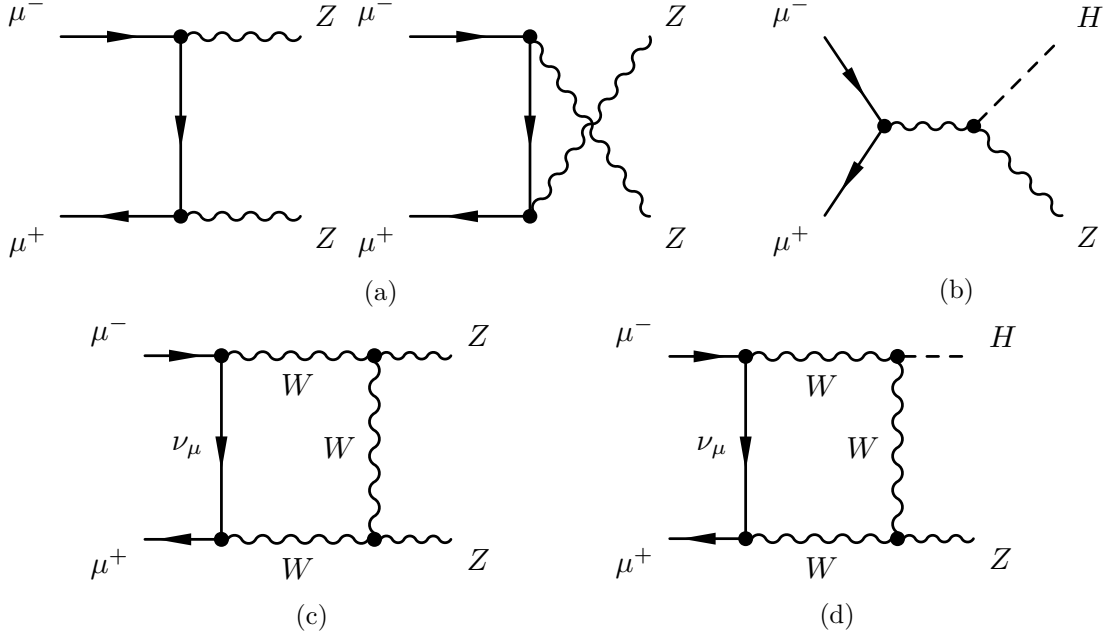


Figure 1: Upper row: tree-level diagrams for the processes $\mu^+\mu^- \rightarrow ZZ$ in (a) and to $\mu^+\mu^- \rightarrow HZ$ (omitting tiny contributions from the muon Yukawa coupling here for simplicity) in (b), respectively. Lower row: representative one-loop diagrams for the virtual contribution to $\mu^+\mu^- \rightarrow ZZ$ in (c) and to $\mu^+\mu^- \rightarrow HZ$ in (d), respectively.

3.1 Collider energy scans for cross sections of HZ and ZZ production

The simplest processes where the effects from fundamental EW higher order perturbative corrections can be understood are neutral di-boson production processes, as these do not feature final-state, but only initial-state QED radiation at NLO in α . These processes have a clear kinematical structure at LO dominated by either s -channel or t/u -channel/peripheral phase space configurations. In Fig. 1 we show the tree-level Feynman diagrams for $\mu^+\mu^- \rightarrow ZZ$ and HZ , respectively, in the upper row. The lower row depicts typical one-loop diagrams, underlining the fact that at the level of NLO EW corrections these processes are closely related. The direct contributions associated with muon-Higgs Yukawa couplings that we always include in the amplitudes in this work, are of very small sizes and always by far subdominant (cf. however [18] for subtle effects of that coupling at very high energies). By scans over \sqrt{s} for LO and NLO inclusive cross sections of HZ and ZZ production at the muon collider, shown in Fig. 2 (upper plot), we can interpret the global behavior of the corrections δ_{EW} (lower plot) to massive neutral gauge boson pair production and Higgsstrahlung processes. The dominant contribution to ZZ production comes from the t -channel diagram displayed in Fig. (1a), and to HZ production from the s -channel diagram in (1b), respectively. This kinematic classification of these processes is useful in order to understand different effects at NLO EW in different kinematic regimes of invariant masses of external particles.

We first discuss the Higgsstrahlung process. In general, this is very similar to the

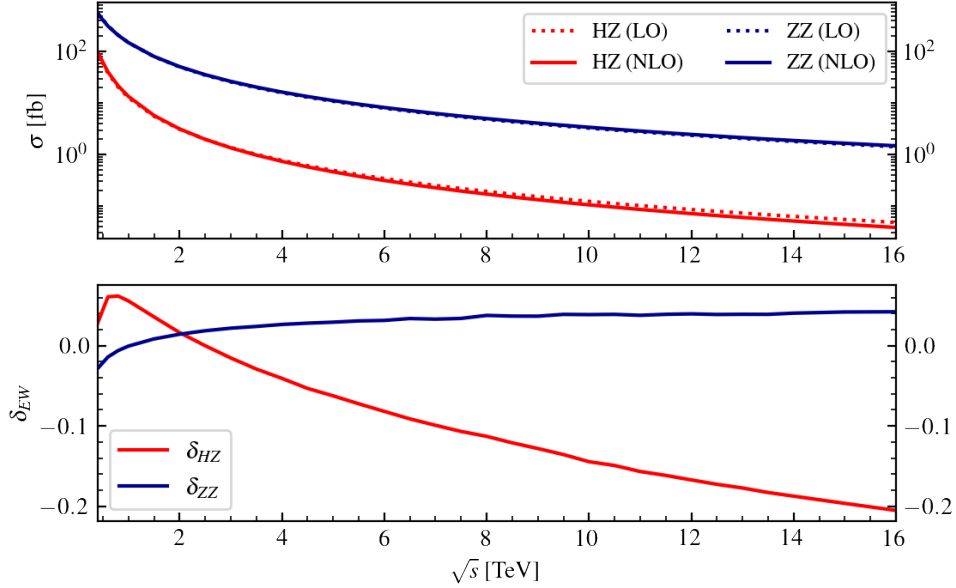


Figure 2: LO and NLO inclusive cross section scans in \sqrt{s} for HZ and ZZ production in the upper plot; relative NLO correction δ_{EW} in the lower plot

corresponding process at an e^+e^- Higgs factory, where NLO QED corrections are known since a long time, even for the off-shell process, $e^+e^- \rightarrow \mu^+\mu^-H$, [38, 39], while leading NLO EW corrections have been calculated in [40]. The on-shell Higgsstrahlung process $e^+e^- \rightarrow ZH$ has recently been also computed at two-loop [41]. However, we are considering the Higgsstrahlung process at the muon collider towards much higher collider energies, where the threshold is only important in radiative return events. For this process, $\mu^+\mu^- \rightarrow HZ$, we observe a large suppression (substantial negative δ_{EW}) in Fig. 2 which increases in size from the peak of the cross section at $\sqrt{s} \sim 0.8$ TeV and which can be attributed to large virtual effects as we will show in the following.

In order to understand the behavior in the regime of high center-of-mass energies, in general we can make use of the approximation of EW Sudakov logarithmic correction factors for which pioneering works have been done in [42–45]. In a kinematic region,

$$r_{kl} = (p_k + p_l)^2 \sim s \gg M_W^2 \quad (3.2)$$

called the Sudakov limit, with k and l arbitrary external states carrying (electro-)weak quantum numbers², these correction factors effectively correspond to the purely EW virtual contributions. Note that in order to restore the full $SU(2)_L \times U(1)_Y$ EW symmetry and to treat all highly-energetic EW gauge bosons equal, one uses a fictitious photon mass $\lambda = M_W$. In addition to the EW virtual corrections, radiative corrections of real photons

²We always assume the multiplicity of external bosons small enough such that the condition Eq. 3.2 is kinematically valid for all external legs simultaneously.

with transverse momenta smaller than a cutoff scale at the order of M_W implicitly are contained in the correction factors.

The high-energy radiative corrections represent form factors in terms of double and single logarithms of the ratio r_{kl}/M_W^2 which are factorized in the soft and/or collinear limit. If we treat the QED IR subtraction in an NLO EW computation exactly, thereby keeping the photon massless as mandated by FKS subtraction, the virtual loop contributions from massive weak vector boson exchange – unlike those of photon exchange – are still regularized by their masses, i. e. the EW scale M_W . Therefore, for large \sqrt{s} , these contributions are implicitly contained in the EW next-to-leading logarithmic (NLL) Sudakov factors. Treating the latter effectively as virtual loop contributions within the FKS scheme is under the caveat that the IR singularities from real emission amplitudes and from loop contributions with photon exchange are regularized at different (inconsistent in the sense of extracting the Sudakov factors) scales. This however can not be circumvented in a trivial way if combining QED FKS subtraction with the Sudakov approximation since for EW $SU(2)_L \times U(1)_Y$ resummation photon exchange in loop contributions cannot be treated separately owing to the mixing in the neutral gauge sector. However, the mismatch of the scales at high energies has minor numerical effects as it is shown by [46].

For illustration, we show in Fig. 2 the logarithmic suppression of the NLO cross section for $\mu^+\mu^- \rightarrow HZ$ in terms of the relative correction δ_{HZ} . In the following, we will show that the effective EW virtual loop contributions of HZ is quantitatively approximated relatively well enough by the Sudakov approach. To this end, we extract the NLL Sudakov form factor for HZ production at the muon collider by using analytical results in an analogous way as for the process $q\bar{q} \rightarrow HZ$ [46]; the technical details and considerations are explained in appendix B, such that we arrive at the estimate of Eq. (B.12). We discuss here only briefly the main features, for more details cf. appendix B. This Sudakov factor as a function of \sqrt{s} for a fixed solid polar angle $\theta = 90^\circ$ (note that the subleading single Sudakov logarithms in Eq. (B.5) are functions of the Mandelstam variables t and u) of the Higgs as shown in Fig. 3 exhibits large suppressions, in particular for left-handed muons in the initial state due to the enhanced $SU(2)_L$ weak interaction coupling. In a further approach we approximated the unpolarized correction factor $\Lambda_{\text{est},c}^{\text{unpol}}$, for which the angular-dependent part of Eq. (B.5) is left out, shown as black dotted curve. This correction factor corresponds to the amount by which at least the inclusive result is suppressed due to the virtual loop corrections. According to Eq. (B.5), the angular-dependent part of the Sudakov factor is negative, of subleading logarithmic type and amounts up to -17% at $\sqrt{s} = 16$ TeV for angles θ_H in the perpendicular plane, i. e. close to 90° . For these angles also the Born process is enhanced according to [47, 48]

$$\left(\frac{d\sigma}{d\Omega}\right)_{\text{Born}} \propto \frac{\beta M_Z^2}{(s - M_Z^2)^2} \left(\frac{s\beta^2}{8M_Z^2} \sin^2 \theta_H + 1 \right) . \quad (3.3)$$

This angular dependence can be observed as well in the differential cross sections for the Born case presented in Sec. 4 within Fig. 8. The estimated unpolarized correction factor, $\Lambda_{\text{est}}^{\text{unpol}}$, given in Eq. (B.16) including the angular-dependent terms, which e.g. for the polar angle $\theta_H = 90^\circ$ decreases the cross section down to -65% , is shown as black dashed curve

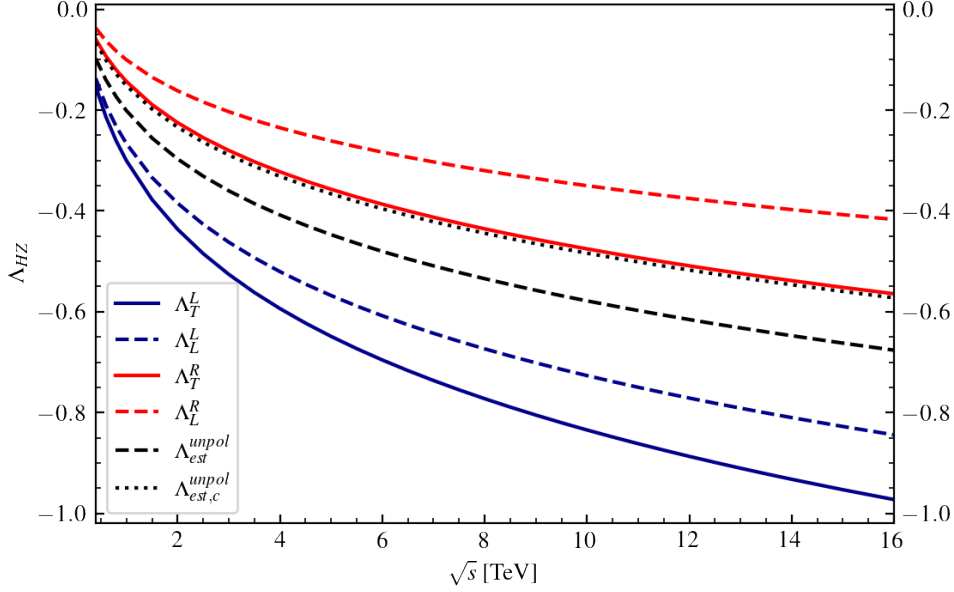


Figure 3: Sudakov factors Λ_λ^κ for muon chiralities $\kappa = L, R$ and Z polarizations $\lambda = T, L$ and estimated unpolarized correction factor $\Lambda_{\text{est}}^{\text{unpol}}$ at $\theta_H = 90^\circ$ as well as $\Lambda_{\text{est},c}^{\text{unpol}}$ (without angular dependent terms) for HZ production at the muon collider as a function of the collider energy, \sqrt{s} .

in Fig. 3. Both, from the magnitude of $\Lambda_{\text{est}}^{\text{unpol}}$ relative to $\Lambda_{\text{est},c}^{\text{unpol}}$ at this angle as well as from a similar enhancement behavior at angles around $\theta_H = 90^\circ$ as for the Born cross section differential in θ_H , the relative inclusive virtual corrections to HZ production can be estimated to be at the order of $\Lambda_{\text{est}}^{\text{unpol}}$. The counteracting effects of QED radiation in an inclusive calculation will be discussed in the following.

By only including pure NLO QED corrections in the calculation, it can be shown that the relative correction δ_{QED} as depicted in Fig. 4 is positive and growing with \sqrt{s} . About the contributing NLO parts we can make the following qualitative statements: In general, virtual loop amplitudes are supposed to give negative contributions such that a positive overall NLO correction factor can be explained by dominating real radiative corrections. In particular, since the main contributions for HZ production at Born-level come from the s-channel diagram, large radiative QED corrections at NLO are expected due to large amplitudes for hard photons radiated in forward direction, the effect of which is enhanced with growing \sqrt{s} . This explains the bulk of the correction factor to be seen in Fig. 4 as the blue curve. From these two effects, the large negative virtual corrections due to EW Sudakov logarithms overcompensate the positive QED radiation effects, resulting in an overall decrease of the cross section of $\delta_{HZ} \sim -20\%$ at high energies in Fig. 2. This magnitude is very reasonable from the general considerations of the size of Sudakov logarithms and the leading logarithm of quasi-collinear photon radiation.

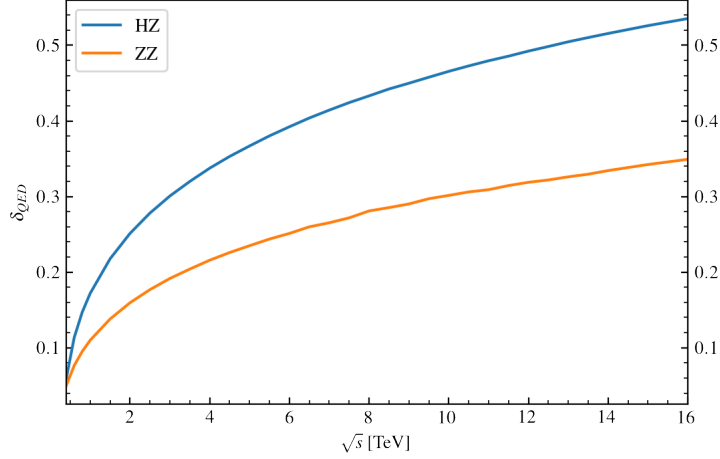


Figure 4: Relative QED corrections $\delta_{QED} = \sigma_{\text{NLO,QED}}^{\text{incl}} / \sigma_{\text{LO}}^{\text{incl}} - 1$ to HZ and ZZ production at the muon collider as a function of the collider energy, \sqrt{s} .

For the second process, $\mu^+\mu^- \rightarrow ZZ$, we refrain from going into a detailed discussion about the composition of pure weak and QED parts of the NLO inclusive corrections since the process is more intricate from its angular dependence at LO as well as at NLO, due to the presence of t and u channel because of the Bose symmetry of the final-state particles. Explicitly, the result for the Sudakov correction factors of the analogous process $e^+e^- \rightarrow ZZ$ given in [43] cannot be straightforwardly related to an estimate for the Sudakov suppression of the integrated result for the virtual corrections. This is due to the completely different angular dependence of the Sudakov factor depicted in Fig. 7 within Ref. [43] which is minimal at angles around 90° compared to the Born amplitudes with the largest contributions in forward and backward direction. Moreover, in agreement with the suppression $\delta_{QED,ZZ}$ relative to $\delta_{QED,HZ}$ in Fig. 4 we can make the general statement that the impact of real emission amplitudes with hard photon radiation on the relative NLO correction is reduced compared to that of HZ production. This is due to the fact that for ZZ production large contributions coming from forward scattering of the Z bosons at high energies are present already at Born-level due to the dominant t -channel process. Furthermore, for the real-emission process in general the number of helicity degrees of freedom of the Z bosons in the final state is increased relative to the Born process. The latter is non-suppressed only for transversely polarized Z bosons for opposite helicities [49]. Summing and integrating over all degrees of freedom in the final state for the real-emission amplitudes and thereby overcompensating the EW Sudakov effects can explain the overall positive correction δ_{ZZ} which can be seen in Fig. 2.

3.2 Total NLO cross sections for multi-boson processes

In the same way as for our specific processes, HZ and ZZ production, NLO EW corrections can be computed for all other possible combinations of two, three and four bosons in the

final state. In this section, we present numerical results of the LO and NLO inclusive cross sections for a large variety of these processes at $\sqrt{s} = 3$ TeV in Table 1. Table 2 and 3 contain the corresponding results for two- and three-boson production at $\sqrt{s} = 10$ and 14 TeV, respectively. We note, that for high center-of-mass energies as well as high EW boson multiplicities, fixed-order perturbation theory for the electroweak interactions become insufficient. For this reason, we omit the computations for four-boson production at $\sqrt{s} = 10$ and 14 TeV which yield meaningful results only by taking appropriate EW higher order resummation approaches, e. g. by soft-collinear effective field theory, into account. Besides the (fixed-order) NLO EW results, cross sections to tree-level processes including both collinear resummation of leading logarithms (LL) of ratios Q^2/m_μ^2 and Gribov resummation of soft radiation to all orders in α , as well as hard-collinear radiation up to $\mathcal{O}(\alpha^3)$ off the initial state are included in this section. Their numerical results are achieved by making use of LL lepton PDFs with its known analytical form presented in [50–52]. For each corresponding collider energy, these results are displayed in Table 4, 5 and 6, respectively, where the relative correction δ_{ISR} is defined as

$$\delta_{\text{ISR}} = \frac{\sigma_{\text{LO+ISR}}^{\text{incl}}}{\sigma_{\text{LO}}^{\text{incl}}} - 1 \quad . \quad (3.4)$$

We note that in the meantime, also NLL lepton PDFs have become available [53–55] which are already implemented in WHIZARD; as its infrastructure within the NLO framework is still in validation, we do not combine our NLO EW cross sections with those. In addition, for high-energy muon colliders also EW PDFs might start to play a phenomenological role [56]. Their effects from the resummation of EW bosons in the initial state are not taken into account here.

We start the discussion with a few general remarks on the LO and NLO EW results. First of all, we observe that for all processes the absolute value of the cross section decreases with \sqrt{s} and with the number of bosons in the final state. Except for pure Higgs final state, these range from $\sim 10^{-4}$ to $\sim 10^2$ fb. Because of the size of the cross sections for the tree-level processes for $\mu^+\mu^- \rightarrow HH$ and $\mu^+\mu^- \rightarrow HHH$ production which is $\lesssim 2 \cdot 10^{-7}$ fb due to the tiny muon-Higgs couplings at the energies far above the 125 GeV threshold, we leave out a detailed discussion on the theoretical background of the shown $\mathcal{O}(\alpha)$ corrections. The abnormally large corrections to cross sections labeled with ‘*’ in in Table 1, 2 and 3 at this fixed order can be related to the fact, that the loop-induced process is of comparable or even larger size than the formally leading tree-level process. Hence, the formal NLO correction to the tree-level process should be rather considered as an interference between the tree-level and the loop-induced process. The square of the one-loop amplitude as part of the loop-induced process is beyond the $\mathcal{O}(\alpha)$ correction predictions considered in this paper and will be deferred to a future publication. However, although not relevant for the center-of-mass energies used for the simulations of this study, for completeness we included the LO and formal NLO $\mu^+\mu^- \rightarrow HH$ and $\mu^+\mu^- \rightarrow HHH$ numerical cross section results in these tables.

For the two specific di-boson processes $\mu^+\mu^- \rightarrow ZZ$ and $\mu^+\mu^- \rightarrow HZ$, we refer to the detailed discussion within the previous chapter and highlight the different kinematical

$\mu^+\mu^- \rightarrow X, \sqrt{s} = 3 \text{ TeV}$	$\sigma_{\text{LO}}^{\text{incl}} [\text{fb}]$	$\sigma_{\text{NLO}}^{\text{incl}} [\text{fb}]$	$\delta_{\text{EW}} [\%]$
W^+W^-	$4.6591(2) \cdot 10^2$	$4.847(7) \cdot 10^2$	+4.0(2)
ZZ	$2.5988(1) \cdot 10^1$	$2.656(2) \cdot 10^1$	+2.19(6)
HZ	$1.3719(1) \cdot 10^0$	$1.3512(5) \cdot 10^0$	-1.51(4)
HH	$1.60216(7) \cdot 10^{-7}$	$5.66(1) \cdot 10^{-7} *$	
W^+W^-Z	$3.330(2) \cdot 10^1$	$2.568(8) \cdot 10^1$	-22.9(2)
W^+W^-H	$1.1253(5) \cdot 10^0$	$0.895(2) \cdot 10^0$	-20.5(2)
ZZZ	$3.598(2) \cdot 10^{-1}$	$2.68(1) \cdot 10^{-1}$	-25.5(3)
HZZ	$8.199(4) \cdot 10^{-2}$	$6.60(3) \cdot 10^{-2}$	-19.6(3)
HHZ	$3.277(1) \cdot 10^{-2}$	$2.451(5) \cdot 10^{-2}$	-25.2(1)
HHH	$2.9699(6) \cdot 10^{-8}$	$0.86(7) \cdot 10^{-8} *$	
$W^+W^-W^+W^-$	$1.484(1) \cdot 10^0$	$0.993(6) \cdot 10^0$	-33.1(4)
W^+W^-ZZ	$1.209(1) \cdot 10^0$	$0.699(7) \cdot 10^0$	-42.2(6)
W^+W^-HZ	$8.754(8) \cdot 10^{-2}$	$6.05(4) \cdot 10^{-2}$	-30.9(5)
W^+W^-HH	$1.058(1) \cdot 10^{-2}$	$0.655(5) \cdot 10^{-2}$	-38.1(4)
$ZZZZ$	$3.114(2) \cdot 10^{-3}$	$1.799(7) \cdot 10^{-3}$	-42.2(2)
$HZZZ$	$2.693(2) \cdot 10^{-3}$	$1.766(6) \cdot 10^{-3}$	-34.4(2)
$HHZZ$	$9.828(7) \cdot 10^{-4}$	$6.24(2) \cdot 10^{-4}$	-36.5(2)
$HHHZ$	$1.568(1) \cdot 10^{-4}$	$1.165(4) \cdot 10^{-4}$	-25.7(2)

Table 1: Total inclusive cross sections at LO and NLO EW with corresponding relative corrections δ_{EW} , for two-, three- and four-boson production at $\sqrt{s} = 3 \text{ TeV}$. For (*), with dominant loop-induced contributions, we refer to the discussion in the text.

$\mu^+\mu^- \rightarrow X, \sqrt{s} = 10 \text{ TeV}$	$\sigma_{\text{LO}}^{\text{incl}} [\text{fb}]$	$\sigma_{\text{NLO}}^{\text{incl}} [\text{fb}]$	$\delta_{\text{EW}} [\%]$
W^+W^-	$5.8820(2) \cdot 10^1$	$6.11(1) \cdot 10^1$	+3.9(2)
ZZ	$3.2730(4) \cdot 10^0$	$3.401(4) \cdot 10^0$	+3.9(1)
HZ	$1.22929(8) \cdot 10^{-1}$	$1.0557(8) \cdot 10^{-1}$	-14.12(7)
HH	$1.31569(5) \cdot 10^{-9}$	$42.9(4) \cdot 10^{-9} *$	
W^+W^-Z	$9.609(5) \cdot 10^0$	$5.86(4) \cdot 10^0$	-39.0(2)
W^+W^-H	$2.1263(9) \cdot 10^{-1}$	$1.31(1) \cdot 10^{-1}$	-38.4(5)
ZZZ	$8.565(4) \cdot 10^{-2}$	$5.27(8) \cdot 10^{-2}$	-38.5(9)
HZZ	$1.4631(6) \cdot 10^{-2}$	$0.952(6) \cdot 10^{-2}$	-34.9(4)
HHZ	$6.083(2) \cdot 10^{-3}$	$2.95(3) \cdot 10^{-3}$	-51.6(5)
HHH	$2.3202(4) \cdot 10^{-9}$	$-1.0(2) \cdot 10^{-9} *$	

Table 2: Total inclusive cross sections at LO and NLO with corresponding relative correction δ_{EW} for di- and tri-boson production at $\sqrt{s} = 10 \text{ TeV}$. For (*), with dominant loop-induced contributions, we refer to remarks in the text.

$\mu^+\mu^- \rightarrow X, \sqrt{s} = 14 \text{ TeV}$	$\sigma_{\text{LO}}^{\text{incl}} [\text{fb}]$	$\sigma_{\text{NLO}}^{\text{incl}} [\text{fb}]$	$\delta_{\text{EW}} [\%]$
W^+W^-	$3.2423(1) \cdot 10^1$	$3.358(8) \cdot 10^1$	+3.6(2)
ZZ	$1.80357(9) \cdot 10^0$	$1.872(4) \cdot 10^0$	+3.8(2)
HZ	$6.2702(4) \cdot 10^{-2}$	$5.097(6) \cdot 10^{-2}$	-18.7(1)
HH	$3.4815(1) \cdot 10^{-10}$	$217.(2) \cdot 10^{-10} *$	
W^+W^-Z	$6.369(3) \cdot 10^0$	$3.51(3) \cdot 10^0$	-45.0(4)
W^+W^-H	$1.2846(6) \cdot 10^{-1}$	$0.73(1) \cdot 10^{-1}$	-43.3(9)
ZZZ	$5.475(3) \cdot 10^{-2}$	$3.06(3) \cdot 10^{-2}$	-44.2(6)
HZZ	$8.754(4) \cdot 10^{-3}$	$5.28(3) \cdot 10^{-3}$	-39.7(4)
HHZ	$3.668(1) \cdot 10^{-3}$	$1.49(1) \cdot 10^{-3}$	-59.4(3)
HHH	$1.1701(2) \cdot 10^{-9}$	$-0.739(8) \cdot 10^{-9} *$	

Table 3: Total inclusive cross sections at LO and NLO with corresponding relative correction δ_{EW} for di- and tri-boson production at $\sqrt{s} = 14 \text{ TeV}$. For (*), with dominant loop-induced contributions, we refer to remarks in the text.

effects of these processes. The W pair production, $\mu^+\mu^- \rightarrow W^+W^-$, despite being different to ZZ at lower energies due to the interference with the s -channel, is similar at higher energies due to dominant contributions from t -channel diagrams at Born level, and also initial-state radiation patterns similar to $\mu^+\mu^- \rightarrow ZZ$. The main differences are the real-emission amplitudes with photon radiation off the final state. This can induce semi-collinear effects in $W\gamma$ splittings which increase with the energy scale of the process. However, this is a minor effect compared to large contributions from semi-collinear photon radiation off the light muons in the initial state. Another difference to ZZ is that the W bosons can have *two* longitudinal gauge boson polarizations corresponding to charged Goldstone bosons in the final state, for which the s -channel process is dominant, but which is suppressed with $1/s$ [57, 58]. These considerations may explain the similarity of the relative corrections δ_{EW} of the two gauge boson pair production processes at high energies 10 and 14 TeV compared to their difference at 3 TeV.

The quantitatively different behavior between gauge boson pair production $\mu^+\mu^- \rightarrow VV$ and Higgsstrahlung $\mu^+\mu^- \rightarrow HZ$ at the considered collider energies can be seen between the fixed-order electroweak correction factors δ_{EW} and the resummed ISR correction factors δ_{ISR} in Tables 4, 5 and 6. According to these, the correction from ISR resummation for $\mu^+\mu^- \rightarrow HZ$ is approximately twice as big as for $\mu^+\mu^- \rightarrow VV$ at 3 TeV and grows with the energy. This can be understood from pure kinematics of the Born processes: Higgsstrahlung is s -channel and falls off with $1/s$, hence ISR induces a radiative return back to the threshold and enhances the cross section at NLO, while for $\mu^+\mu^- \rightarrow VV$ the t -channel dominates and damps the $1/s$ fall-off by a logarithmic correction towards $\log(s)/s$. Hence, the radiative return is less prominent for the EW diboson production. Speaking differently, the large positive $\mathcal{O}(\alpha \ln(Q^2/m_\mu^2))$ logarithms due to hard collinear photon ISR are enhanced with the collider energy and induce a boost of the photon recoil system along the beam axis. This causes a forward scattering of the final state massive HZ system and thus semi-collinear effects in high energy regions of the phase space.

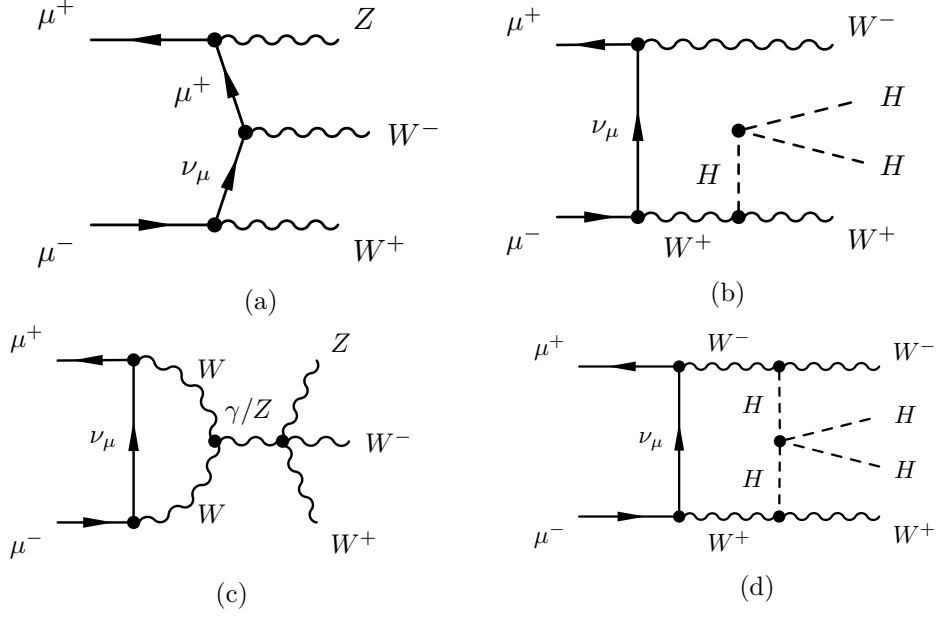


Figure 5: Upper row: tree-level diagrams for the processes $\mu^+ \mu^- \rightarrow W^+ W^- Z$ in (a) and to $\mu^+ \mu^- \rightarrow W^+ W^- H H$ in (b), respectively. Lower row: representative one-loop diagrams for the virtual contribution to $\mu^+ \mu^- \rightarrow W^+ W^- Z$ in (c) and to $\mu^+ \mu^- \rightarrow W^+ W^- H H$ in (d), respectively.

We now turn to processes of higher multiplicities, with three and four EW gauge and/or Higgs bosons in the final state, again omitting processes with only Higgs bosons in the final state. Fig. 5 shows the Feynman diagrams for the two processes $\mu^+ \mu^- \rightarrow W^+ W^- Z$ and $\mu^+ \mu^- \rightarrow W^+ W^- H H$, respectively. The upper row shows a typical tree-level diagrams, while in the lower row representative one-loop diagrams are shown, which include e.g. quartic gauge or Higgs couplings.

For the triple-boson processes at 3 TeV, we observe a suppression of -20% to -25% of the NLO EW cross section relatively to the LO result, summarized in Table 1. Compared to the small absolute value of δ_{EW} of the di-boson processes, this behavior is due to the fact that negative Sudakov logarithm factors add up for all external states in kinematic regimes where the Sudakov limit, Eq. (3.2), is fulfilled [44]. For four-boson final states, this effect is further enhanced, seen by δ_{EW} ranging from -26% to -42% . In addition, it can be seen from Table 4, 5 and 6 that with increasing number of bosons in the final state the enhancement due to ISR effects decreases. This comes from the multi-peripheral kinematics of these hard processes, similar to what was described above for the diboson processes: the radiative return is not so much pronounced as there is not a single dominating threshold to return to. Consequently, the dominant contribution to the full NLO EW correction δ_{EW} for three-boson final states and nearly the complete contribution of δ_{EW} for the four-boson processes is purely due to negative EW virtual final state correction factors.

After all, a pattern for the relative NLO EW correction δ_{EW} at 3 TeV for the two- and three-boson production processes emerges, which is directly related to their kinematical

$\mu^+\mu^- \rightarrow X, \sqrt{s} = 3 \text{ TeV}$	$\sigma_{\text{LO}}^{\text{incl}} [\text{fb}]$	$\sigma_{\text{LO+ISR}}^{\text{incl}} [\text{fb}]$	$\delta_{\text{ISR}} [\%]$
W^+W^-	$4.6591(2) \cdot 10^2$	$5.303(2) \cdot 10^2$	+13.82(4)
ZZ	$2.5988(1) \cdot 10^1$	$3.007(1) \cdot 10^1$	+15.71(4)
HZ	$1.3719(1) \cdot 10^0$	$1.7868(4) \cdot 10^0$	+30.24(3)
W^+W^-Z	$3.330(2) \cdot 10^1$	$3.427(2) \cdot 10^1$	+2.90(9)
W^+W^-H	$1.1253(5) \cdot 10^0$	$1.2052(7) \cdot 10^0$	+7.10(8)
ZZZ	$3.598(2) \cdot 10^{-1}$	$3.786(2) \cdot 10^{-1}$	+5.24(8)
HZZ	$8.199(4) \cdot 10^{-2}$	$8.887(5) \cdot 10^{-2}$	+8.39(8)
HHZ	$3.277(1) \cdot 10^{-2}$	$3.525(2) \cdot 10^{-2}$	+7.58(7)
$W^+W^-W^+W^-$	$1.484(1) \cdot 10^0$	$1.465(1) \cdot 10^0$	-1.3(1)
W^+W^-ZZ	$1.209(1) \cdot 10^0$	$1.187(1) \cdot 10^0$	-1.8(1)
W^+W^-HZ	$8.754(8) \cdot 10^{-2}$	$8.742(8) \cdot 10^{-2}$	-0.1(1)
W^+W^-HH	$1.058(1) \cdot 10^{-2}$	$1.076(1) \cdot 10^{-2}$	+1.7(1)
$ZZZZ$	$3.114(2) \cdot 10^{-3}$	$3.139(3) \cdot 10^{-3}$	+0.8(1)
$HZZZ$	$2.693(2) \cdot 10^{-3}$	$2.730(2) \cdot 10^{-3}$	+1.4(1)
$HHZZ$	$9.828(7) \cdot 10^{-4}$	$10.042(8) \cdot 10^{-4}$	+2.2(1)
$HHHZ$	$1.568(1) \cdot 10^{-4}$	$1.657(1) \cdot 10^{-4}$	+5.7(1)

Table 4: Total inclusive cross sections at LO with LL ISR photon resummation, and including relative correction δ_{ISR} for two-, three- and four-boson production at $\sqrt{s} = 3$ TeV.

$\mu^+\mu^- \rightarrow X, \sqrt{s} = 10 \text{ TeV}$	$\sigma_{\text{LO}}^{\text{incl}} [\text{fb}]$	$\sigma_{\text{LO+ISR}}^{\text{incl}} [\text{fb}]$	$\delta_{\text{ISR}} [\%]$
W^+W^-	$5.8820(2) \cdot 10^1$	$7.295(7) \cdot 10^1$	+24.0(1)
ZZ	$3.2730(4) \cdot 10^0$	$4.119(4) \cdot 10^0$	+25.8(1)
HZ	$1.22929(8) \cdot 10^{-1}$	$1.8278(5) \cdot 10^{-1}$	+48.69(4)
W^+W^-Z	$9.609(5) \cdot 10^0$	$10.367(8) \cdot 10^0$	+7.9(1)
W^+W^-H	$2.1263(9) \cdot 10^{-1}$	$2.410(2) \cdot 10^{-1}$	+13.3(1)
ZZZ	$8.565(4) \cdot 10^{-2}$	$9.431(7) \cdot 10^{-2}$	+10.1(1)
HZZ	$1.4631(6) \cdot 10^{-2}$	$1.677(1) \cdot 10^{-2}$	+14.62(8)
HHZ	$6.083(2) \cdot 10^{-3}$	$6.916(3) \cdot 10^{-3}$	+13.68(6)

Table 5: Total inclusive cross sections at LO with LL ISR photon resummation and relative correction δ_{ISR} for two- and three-boson production at $\sqrt{s} = 10$ TeV.

structure and remains valid for the results at 10 and 14 TeV. The same reasoning as for the diboson processes $\mu^+\mu^- \rightarrow VV$ can be attributed to NLO correction factors with approximately the same size for $\mu^+\mu^- \rightarrow WWZ, WWH, ZZZ$ and HZZ , respectively, which can be seen at all energies in the tables. The most reasonable explanation is that the bulk of their NLO contributions comes from t -channel diagrams with at least two gauge bosons in the final state which induce enhanced Born and real amplitudes for small scattering angles and high final state momenta (forward scattering). This is different to the Drell-Yan-like Higgs- and di-Higgsstrahlung processes, i. e. HZ and HHZ production, for which the former compared to WW/ZZ and the latter compared to $WWH/WWZ/ZZZ/ZZH$

$\mu^+\mu^- \rightarrow X, \sqrt{s} = 14 \text{ TeV}$	$\sigma_{\text{LO}}^{\text{incl}} [\text{fb}]$	$\sigma_{\text{LO+ISR}}^{\text{incl}} [\text{fb}]$	$\delta_{\text{ISR}} [\%]$
W^+W^-	$3.2423(1) \cdot 10^1$	$4.162(4) \cdot 10^1$	+28.4(1)
ZZ	$1.80357(9) \cdot 10^0$	$2.288(1) \cdot 10^0$	+26.86(6)
HZ	$6.2702(4) \cdot 10^{-2}$	$9.692(3) \cdot 10^{-2}$	+54.57(5)
W^+W^-Z	$6.369(3) \cdot 10^0$	$6.961(6) \cdot 10^0$	+9.3(1)
W^+W^-H	$1.2846(6) \cdot 10^{-1}$	$1.477(1) \cdot 10^{-1}$	+14.98(9)
ZZZ	$5.475(3) \cdot 10^{-2}$	$6.110(5) \cdot 10^{-2}$	+11.6(1)
HZZ	$8.754(4) \cdot 10^{-3}$	$10.197(7) \cdot 10^{-3}$	+16.49(9)
HHZ	$3.668(1) \cdot 10^{-3}$	$4.237(2) \cdot 10^{-3}$	+15.51(7)

Table 6: Total inclusive cross sections at LO with LL ISR photon resummation and relative correction δ_{ISR} for two- and three-boson production at $\sqrt{s} = 14 \text{ TeV}$.

have distinct δ_{EW} of -15% to -20% in table 2 and 3. This observation can be related to the behavior of δ_{HZ} compared to δ_{ZZ} with \sqrt{s} in Fig. 2 for which a detailed study is given in section 3.1. Concluding, the kinematical structure, either t - or s -channel, of the dominant Born process has a decisive impact on the relative size of NLO EW corrections to inclusive cross sections.

4 Differential distributions for NLO EW corrections

In order to give an overview on the impact of NLO EW corrections on differential observables, we produce differential distributions for the process $\mu^+\mu^- \rightarrow HZ$ at $\sqrt{s} = 3, 10$ and 14 TeV , respectively, for different Higgs observables which are displayed in Fig. 6, 7 and 8, respectively. Obviously, these are fixed-order NLO differential distributions which for realistic physics simulation would require a proper matching to QED parton showers in order to describe all of the electromagnetic activity in the event, which we do not attempt in this paper. However, we do investigate the effects of EW corrections on observables for which cuts on the fiducial phase space are imposed. In particular, for this case, phase space points with hard photons exceeding a certain energy are considered as observable photons and hence are discarded in the analysis. This is along the lines of typical experimental analyses at high-energy lepton colliders like ILC [59]. In order to visualize the impact of this phase-space cut, we show – together with the corresponding Born observable – two curves for the NLO observables, one for the case that no cuts are imposed on photon radiation, called ‘NLO-no-cuts’, and a veto on (very) hard photons,

$$E_\gamma < 0.7 \cdot \sqrt{s}/2, \quad (4.1)$$

which we dub ‘NLO-cuts’ (as there is no QED radiation at the level of the Born process, such a cut is trivial at LO).

We show distributions for cross sections differential in the Higgs transverse momentum, $p_{T,H}$, for the three different center-of-mass energies, 3, 10, and 14 TeV , respectively, in Fig. 6. In these plots we see that the differential K factor, i.e the ratio of NLO over Born differential cross section is mostly constant for low $p_{T,H}$ values, reaches a maximum of

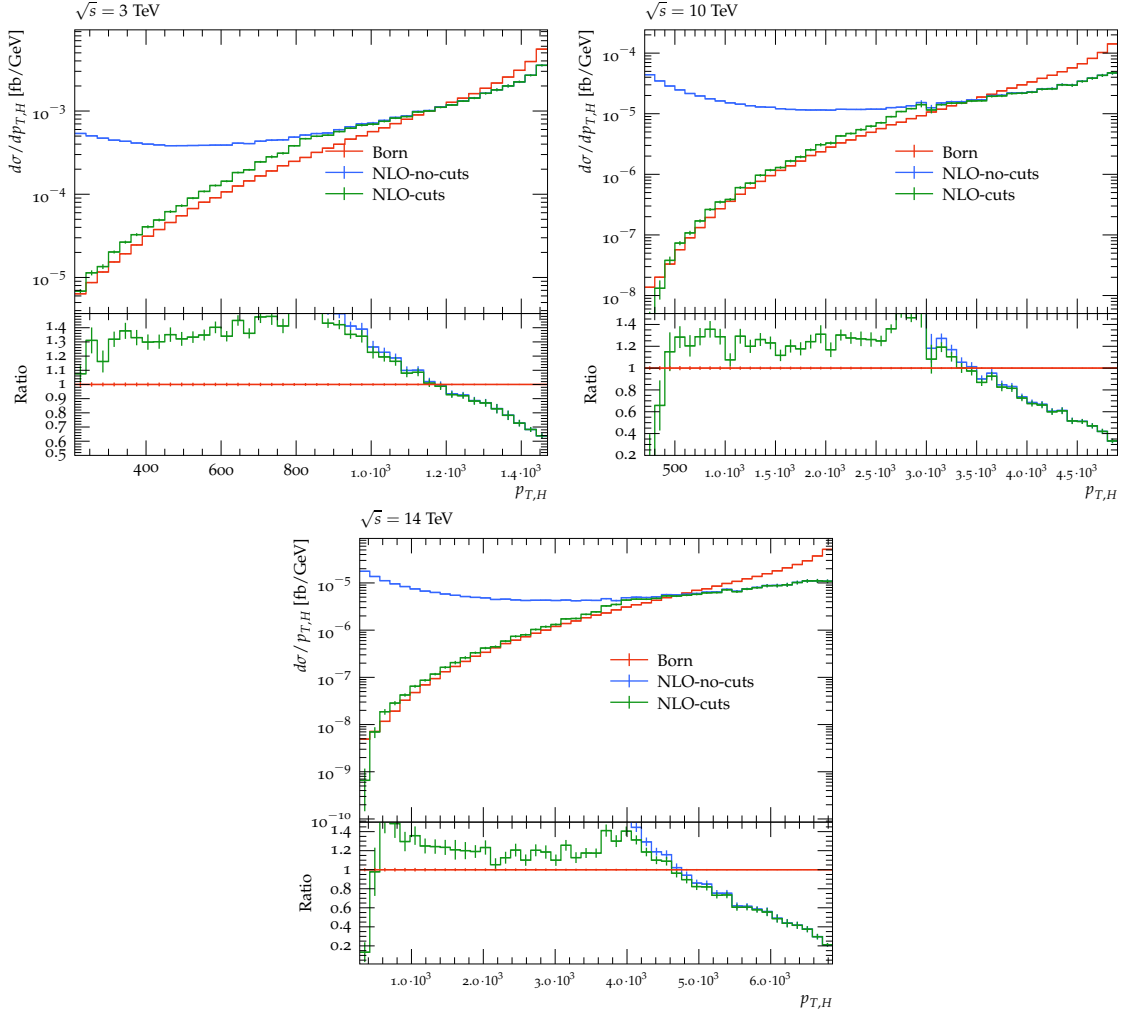


Figure 6: Higgs transverse momentum distributions, $d\sigma/dp_{T,H}(\mu^+\mu^- \rightarrow HZ)$, at $\sqrt{s} = 3$, 10 and 14 TeV, respectively.

roughly 1.5-1.6 and then decreases steeply for $\sqrt{s}/4 \lesssim p_{T,H} \lesssim \sqrt{s}/2$. In this part of the $p_{T,H}$ range, the curves ‘NLO-no-cuts’ and ‘NLO-cuts’ almost coincide, and the decrease of the ratio is steeper the larger the collider energy is, i. e. the differential K factor drops to ~ 0.6 for $\sqrt{s} = 3$ TeV, ~ 0.4 for $\sqrt{s} = 10$ TeV and ~ 0.2 for $\sqrt{s} = 14$ TeV, respectively.

Again, the origin of this large negative corrections can be traced back to EW Sudakov logarithmic factors in the form of $\log^2[p_{HZ}^2/M_W^2]$, which grow with the invariant mass of Born HZ Higgsstrahlung system. Obviously, this behavior gets enhanced the larger the center-of-mass energy of the process is.

The cut on the photon energy influences the differential distributions in regions which are kinematically not accessible at Born level and hence receive so-called huge (differential) K factors. This happens in the region where the Higgs boson has rather small transverse momentum, $p_{T,H} \lesssim \frac{1}{2} p_{T,H}^{\max}$, as it recoils at Born level against the Z . This region is then filled by hard photon radiation at NLO; the veto of Eq. (4.1) on such hard radiation

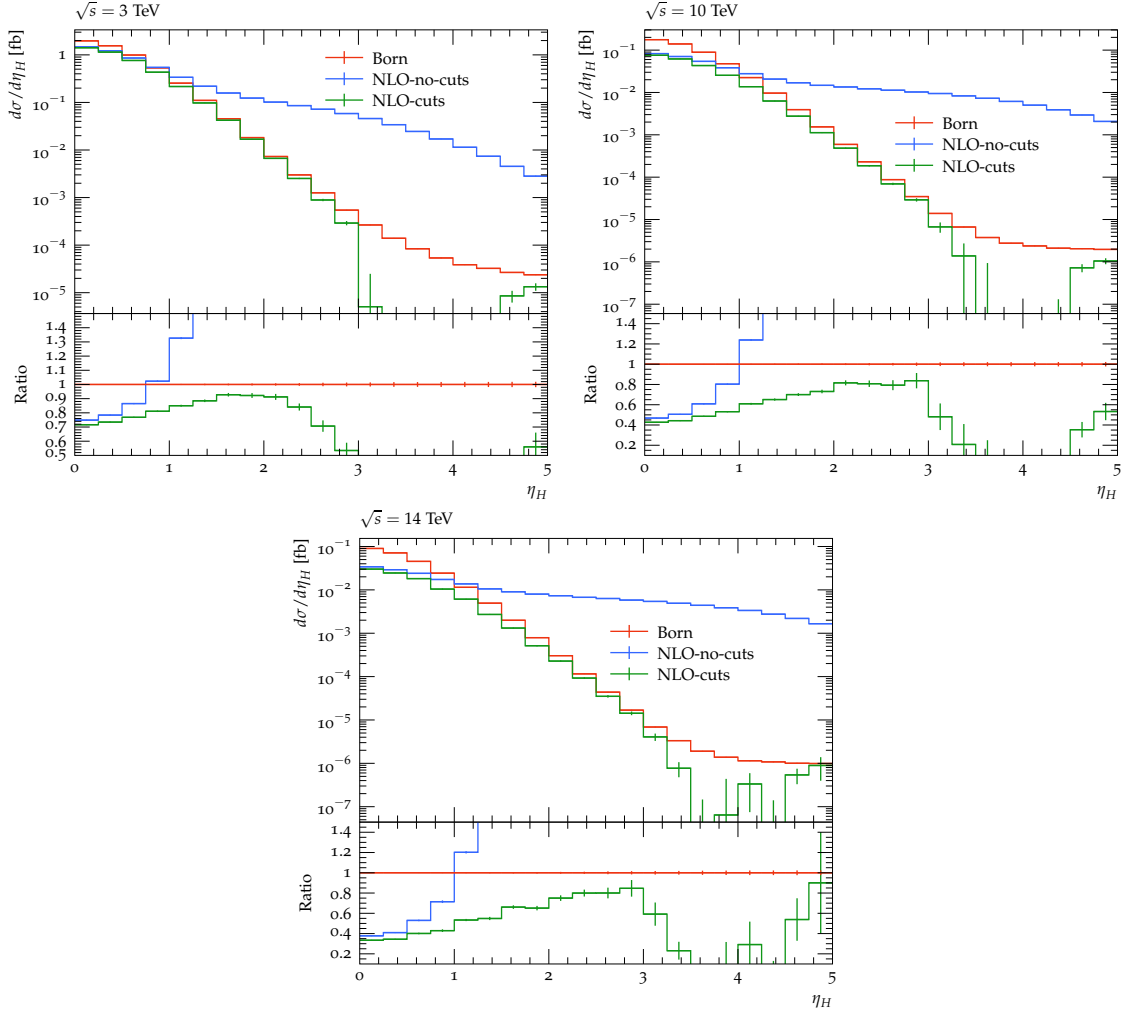


Figure 7: Higgs pseudorapidity distributions, $d\sigma/d\eta_H(\mu^+\mu^- \rightarrow HZ)$, at $\sqrt{s} = 3, 10$ and 14 TeV, respectively. The distributions are symmetric in η_H .

reduces the differential K factors to moderate values of ~ 1.2 . These radiative tails enhance especially the lowest bins in the $p_{T,H}$ distribution by two, or for $\sqrt{s} = 14$ TeV even three orders of magnitude. Using hadron-collider language, such events would rather fall into exclusive ZH plus n "jet" bins, $\mu^+\mu^- \rightarrow ZH + n\gamma$. As for jet vetoes at the LHC, for such hard photon radiation, a QED resummation is necessary to give a reliable estimate on the theoretical uncertainty of the prediction in these parts of the phase space.

Next, we turn to the Higgs pseudorapidity distribution, $d\sigma/d\eta_H(\mu^+\mu^- \rightarrow HZ)$. We make use of the fact that these distributions are symmetric with respect to the central axis of the detector, and so we depicted distributions as a function of the modulus of the Higgs pseudorapidity $|\eta_H|$ for the proposed collider energies in Fig. 7. First of all, we note that the most significant deviation between the full and the "vetoed" NLO distributions in each of the plots is at large pseudorapities, where the Higgs boson recoils against a hard photon emitted collinear to the beam axes. In that regime, real matrix elements are

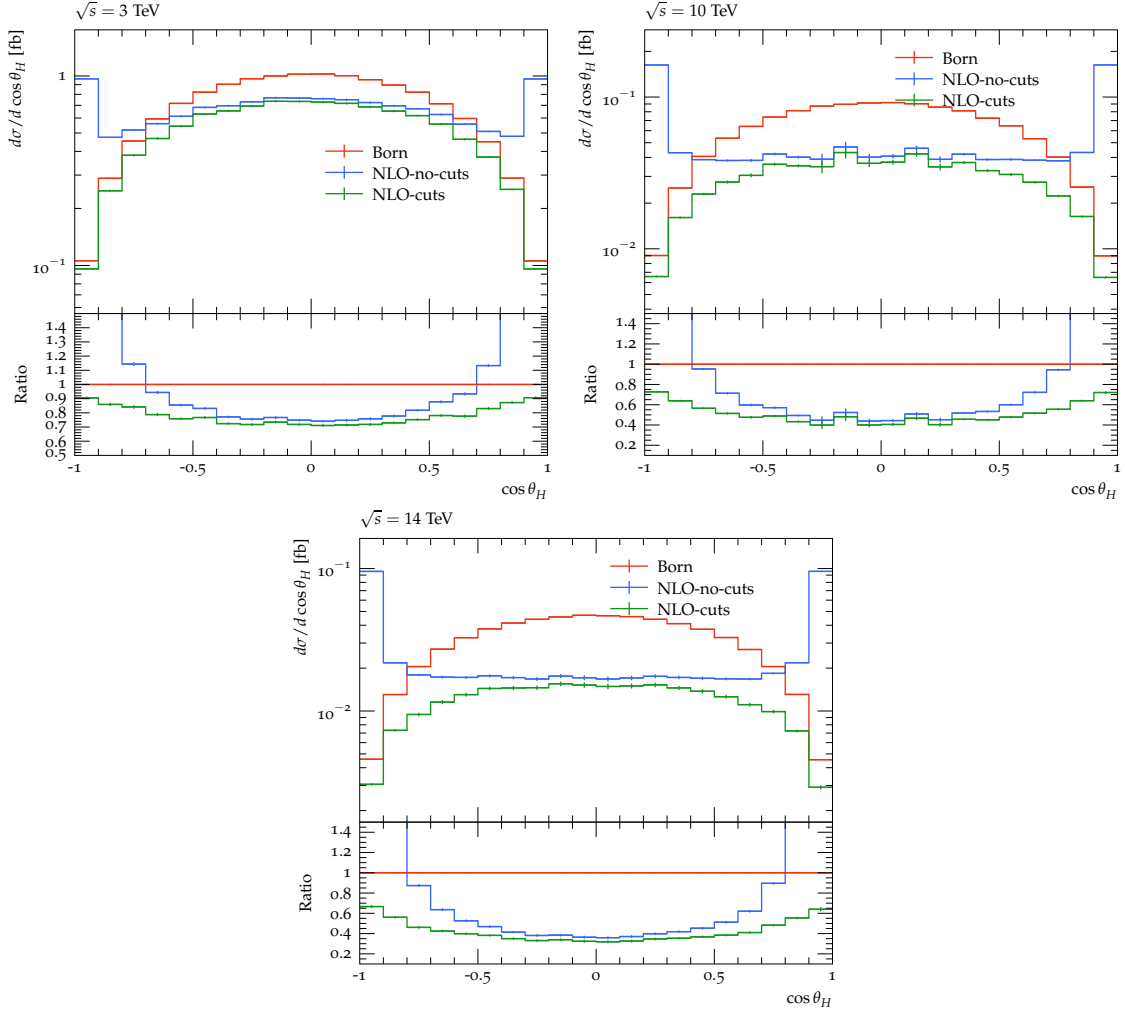


Figure 8: Differential Higgs polar angle distributions, $d\sigma/d\cos\theta_H(\mu^+\mu^-\rightarrow HZ)$ at $\sqrt{s}=3, 10$ and 14 TeV, respectively.

drastically enhanced. On the other hand, for small $|\eta_H|$, real photon radiation for the NLO distributions is suppressed and virtual effects play a much more significant role. For $|\eta_H|=0$, the Higgs is radiated in the plane perpendicular to the beam axis such that the value of the differential K factor reduced by one, $K-1$, is directly comparable to the Sudakov suppression factor $\Lambda_{\text{est}}^{\text{unpol}}$ of Eq. (B.16); this factor is shown in Fig. 3. In fact, the relative deviation of the NLO differential cross section for which cuts are applied of the Born one agrees with $\Lambda_{\text{est}}^{\text{unpol}}$ in the first bin for all the shown plots at the level of a few percent.

Almost the same physics like in the pseudorapidity distributions is encoded in the differential distributions for the Higgs polar angle, $d\sigma/d\cos\theta_H(\mu^+\mu^-\rightarrow ZH)$. However, the polar angle distributions are much more common for Higgs studies at lepton colliders. We show the Higgs polar angle distributions for our three different collider energies of 3, 10 and 14 TeV, respectively, in Fig. 8. Again, one observes that the bulk of the Born

contribution is located at the central part of the detector around $\theta_H = 90^\circ$. This can be understood from the $\sin^2 \theta_H$ dependence of amplitudes with longitudinally polarized Z bosons which are enhanced by s/M_Z^2 compared to transversal ones [48]. By comparing the curves labelled "NLO-no-cuts" and "NLO-cuts" one sees again that the photon veto, Eq. (4.1), cuts out the collinearly strongly enhanced emission along the beam directions. For angles in the central part of the phase space, the cut has only a minor effect and the two curves deviate only at a few percent. As in the case for the central description in terms of the pseudorapidity, $\eta_H \sim 0$, the Sudakov factor $\Lambda_{\text{est}}^{\text{unpol}}$ can be found to be an accurate approximation for $d\sigma/d\cos\theta_H$ at $\theta_H = \pi/2$, especially for high collider energy and when applying a hard photon veto.

It would be interesting to also study differential distributions for production processes with two, three and four electroweak gauge bosons. However, this chapter served mostly as a proof of principle and we leave such dedicated studies for future publications [60].

5 Conclusions and Outlook

In this paper, we have presented the – to our knowledge – first systematic set of calculations of NLO EW corrections to the production of two, three and four electroweak gauge and Higgs bosons at a future high-energy muon collider at three different collider energies of 3, 10 and 14 TeV. Such a collider has recently regained a lot of interest not as a Higgs factory, but as a machine at the utmost energy frontier, particularly along the lines of the US Snowmass Community Study 2021. In order to map out the full physics potential of such a collider, especially with respect to the discovery reach for new physics, it is crucial to have precision predictions for SM processes at hand. We studied a quite extensive list of processes including two, three and four Higgs and/or electroweak vector bosons at fixed NLO EW as well as with QED ISR leading-logarithmic collinear resummation. Processes with only Higgs bosons in the final state are special, as they are highly suppressed at tree level due to the tiny muon Yukawa coupling; the tree-level matrix element is of the same order or even smaller than the one-loop matrix element, such that the normal loop-wise expansion is not meaningful here. For the other multi-boson processes, $\mu^+\mu^- \rightarrow V^n H^m, n+m \leq 4, n \neq 0$, the results presented in this work reflect two significant features of the higher order EW corrections: on the one hand, large negative virtual corrections from EW Sudakov double (and single) logarithms, and on the other hand large collinear logarithms from initial-state photon radiation. Generically, for all processes the negative EW Sudakov factors overcompensate for the enhancement of real contributions from hard photon ISR with the exception of the diboson processes $\mu^+\mu^- \rightarrow VV$.

The suppression of NLO EW inclusive cross sections with respect to the LO results range down from -20% for three bosons at 3 TeV and to about -60% for three bosons at 14 TeV. Furthermore, Higgs- and multi-Higgsstrahlung processes exhibit much smaller suppression rates compared to other multi-boson processes at high energies. This is due to their s -channel dominated kinematical structure which allows the resummed ISR collinear radiation a much stronger enhancement from radiative return.

We also presented results for NLO fixed-order differential distributions, as a showcase for the process $\mu^+\mu^- \rightarrow HZ$. For this process, we did an extensive comparison of such differential distributions to the pure EW NLL Sudakov factor approximation, and find very good agreement, e.g. the suppression of $d\sigma/d\cos\theta_H$ in distributions for Higgs polar angles perpendicular to the beam axis. These comparisons also include angular-dependent (subleading, i.e. single-logarithmic) Sudakov factors. These factors even more accurately describe the suppression of the distributions if very hard photon radiation is vetoed by a cut on the radiated photon energy of $E_\gamma < 0.7\sqrt{s}$. This regime of the phase space should be considered as part of the exclusive photon "jet" bins, $\mu^+\mu^- \rightarrow HZ + n\gamma$.

There are several further roads to pursue from here: for a universal treatment of collinear ISR effects in the NLO EW calculation next-to-leading logarithmic (NLL) collinear initial-state resummation must be applied by factorizing lepton PDFs at this accuracy level. This would allow to systematically combine the two different types of corrections properly. In our simulation framework, this is work in progress and will be available in the future. Such a theoretical description mandates treating the initial-state muons as massless. Care has then to be taken when effects from Higgs radiation off massive muon lines are taken into account for multi-Higgs or multi-Higgstrahlung processes. One class of electroweak processes that we have not considered so far, are vector-boson fusion (VBF) or vector-boson scattering (VBS) like processes, which also are of high phenomenological importance. Such processes have to be treated as well with great care, as the quasi-collinear forward neutrinos (for charged currents) and muons (for neutral currents) can only be kinematically, but not conceptually distinguished from decays of single vector bosons. This is beyond the scope of this paper. Finally, in order to be able to study detector effects and systematic uncertainties, unweighted event samples fully matched to initial- and final state photon showers (or at very high energies even EW showers) have to be available. We leave this as well for future work.

Acknowledgments

For stimulating discussions on muon colliders and NLO calculations, we would like to thank Tao Han, Yang Ma and Keping Xie. Furthermore, we give thanks to Adrian Signer for useful advices on QED fixed order computations associated with massive initial state leptons, and to Stefan Kallweit for many helpful details for using `RECOLA` for electroweak corrections. We thank Jonas Lindert for providing corresponding `OpenLoops` process libraries. We also appreciate valuable discussions with Stefano Frixione on theoretical description of initial-state radiation, as well as Mikael Berggren on the treatment of photons in experimental lepton collider analyses. PB, JRR, and PS acknowledge the support by the Deutsche Forschungsgemeinschaft (DFG, German Research Association) under Germany's Excellence Strategy-EXC 2121 "Quantum Universe"-3908333. WK was supported in part by the Deutsche Forschungsgemeinschaft (DFG, German Research Foundation) under grant 396021762 - TRR 257. This work is also been funded by the Deutsche Forschungsgemeinschaft (DFG, German Research Foundation) - 491245950.

A Validation for massive lepton-initiated process setup

For the validation of the WHIZARD+RECOLA setup for simulating cross sections of lepton collider processes at NLO EW we used the input parameters and reference results of [37] for the process $e^+e^- \rightarrow HZ$ with unpolarized beams and massive initial state. A comparison of these checks for different collider energies, i. e. 250, 500 and 1000 GeV, is shown in table 7 below. Note that the shown precisions are not theory uncertainties but just Monte Carlo integration errors which have been chosen to find well enough agreement between the two programs at both LO and NLO.

\sqrt{s} [GeV]	MCSANCee[37]		WHIZARD+RECOLA			$\sigma^{\text{sig}} \text{ (LO/NLO)}$
	$\sigma_{\text{LO}}^{\text{tot}}$ [fb]	$\sigma_{\text{NLO}}^{\text{tot}}$ [fb]	$\sigma_{\text{LO}}^{\text{tot}}$ [fb]	$\sigma_{\text{NLO}}^{\text{tot}}$ [fb]	δ_{EW} [%]	
250	225.59(1)	206.77(1)	225.60(1)	207.0(1)	-8.25	0.4/2.1
500	53.74(1)	62.42(1)	53.74(3)	62.41(2)	+16.14	0.2/0.3
1000	12.05(1)	14.56(1)	12.0549(6)	14.57(1)	+20.84	0.5/0.5

Table 7: Comparison of LO and NLO total inclusive cross sections results of the MCSANCee and WHIZARD+RECOLA setup for the unpolarized process $e^+e^- \rightarrow HZ$

B Derivation of the HZ Sudakov correction factor

We derive the analytic form of the NLL EW Sudakov correction factor to $\mu^+\mu^- \rightarrow HZ$ by applying the general factorization formalism of [43, 44]. Due to the same EW coupling behavior in one-loop processes of $f\bar{f} \rightarrow HZ$ for fermions $f \neq t$, neglecting all masses m_f , and taking into account the explicit values of the electric charges Q_f , this is in analogy to the results of the generic flavor- and chirality-dependent formulae to $q\bar{q} \rightarrow HZ$ in [46]. For $s \gg M_W$ – using the following abbreviations for the double and single logarithmic factors,

$$L(s, M_W^2) = \frac{\alpha}{4\pi} \log^2 \frac{s}{M_W^2} \quad l(s, M_W^2) = \frac{\alpha}{4\pi} \log \frac{s}{M_W^2} \quad , \quad (\text{B.1})$$

we can approximate the leading logarithmic, angular-independent, terms coming from exchange of soft-collinear gauge bosons between pairs of external legs, by the term containing double-logarithmic, single-logarithmic and non-logarithmic contributions,

$$\Lambda_{l,\lambda}^\kappa = A_\lambda^\kappa L(s, M_W^2) + B_\lambda^\kappa \log \frac{M_Z^2}{M_W^2} l(s, M_W^2) + C_\lambda \quad . \quad (\text{B.2})$$

Here, $\lambda = T, L$ denote the transverse and longitudinal polarized Z boson, and $\kappa = L, R$ the muon initial state chirality, respectively. The constant parameters depend on the quantum numbers of the external particles and read

$$A_T^\kappa = -\frac{1}{2} \left[2C_{\mu^\kappa}^{ew} + C_\Phi^{ew} + C_{ZZ}^{ew} \right] \quad A_L^\kappa = - \left[C_{\mu^\kappa}^{ew} + C_\Phi^{ew} \right] \quad (\text{B.3a})$$

$$B_T^\kappa = 2(I_{\mu^\kappa}^Z)^2 + (I_H^Z)^2 \quad B_L^\kappa = 2 \left[(I_{\mu^\kappa}^Z)^2 + (I_H^Z)^2 \right] \quad (\text{B.3b})$$

$$C_T = \delta_H^{LSC,h} \quad C_L = \delta_H^{LSC,h} + \delta_\chi^{LSC,h} \quad . \quad (\text{B.3c})$$

EW Casimir operators C^{ew} as well as explicit values for $(I^Z)^2$ and $\delta^{LSC,h}$ are extracted from [61] and are given by

$$C_{\mu^L}^{ew} = C_{\Phi}^{ew} = \frac{1 + 2c_w^2}{4s_w^2 c_w^2} \quad C_{\mu^R}^{ew} = \frac{1}{c_w^2} \quad C_{ZZ}^{ew} = 2 \frac{c_w^2}{s_w^2} \quad (\text{B.4a})$$

$$(I_{\mu^L}^Z)^2 = \frac{(c_w^2 - s_w^2)^2}{4s_w^2 c_w^2} \quad (I_{\mu^R}^Z)^2 = \frac{s_w^2}{c_w^2} \quad (I_H^Z)^2 = \frac{1}{4s_w^2 c_w^2} \quad (\text{B.4b})$$

$$\delta_H^{LSC,h} = \frac{\alpha}{8\pi s_w^2} \cdot \left[\frac{1}{2c_w^2} \ln^2 \left(\frac{M_H^2}{M_Z^2} \right) + \ln^2 \left(\frac{M_H^2}{M_W^2} \right) \right] \quad (\text{B.4c})$$

$$\delta_{\chi}^{LSC,h} = \frac{\alpha}{16\pi s_w^2 c_w^2} \cdot \ln^2 \left(\frac{M_H^2}{M_Z^2} \right) \quad (\text{B.4d})$$

In the same context, subleading, angular-dependent, terms proportional to $l(s, M_W) \log(|t|/s)$ and $l(s, M_W^2) \log(|u|/s)$ due to W^\pm connecting initial- and final-state legs arise. For the considered Higgsstrahlung process, they take the form³

$$\Lambda_{\theta,\lambda}^\kappa = -\delta_{\kappa L} \frac{D_\lambda}{I_{\mu_\kappa}^Z} l(s, M_W^2) \left[\log \frac{|t|}{s} + \log \frac{|u|}{s} \right] \quad (\text{B.5})$$

with constants

$$D_T = -\frac{c_w(1 + c_w^2)}{2s_w^2} \quad D_L = -\frac{c_w}{s_w} \quad , \quad (\text{B.6})$$

using the shortcuts $s_w = \sin \theta_W$ and $c_w = \cos \theta_W$. Considering the Mandelstam variables t and u in the high energy limit

$$t = (p_{\mu^+} - p_H)^2 \sim -\frac{s}{2}(1 - \cos \theta_H) \quad u = (p_{\mu^+} - p_Z)^2 \sim -\frac{s}{2}(1 + \cos \theta_H) \quad , \quad (\text{B.7})$$

Eq. (B.5) can be written in terms of the Higgs polar angle θ_H . Single-logarithmic terms $\Lambda_{s,\lambda}^\kappa$ originating from virtual soft/collinear gauge bosons emitted from single external legs (wave-function renormalization diagrams) and $\Lambda_{\text{PR},\lambda}^\kappa$ from renormalization of coupling parameters can be expressed as

$$\Lambda_{s,\lambda}^\kappa = E_{s,\lambda}^\kappa l(s, M_W^2) + \frac{\alpha}{4\pi} F_{s,\lambda}^\kappa \quad \Lambda_{\text{PR},\lambda}^\kappa = E_{\text{PR},\lambda}^\kappa l(s, M_W^2) + \frac{\alpha}{4\pi} F_{\text{PR},\lambda}^\kappa \quad , \quad (\text{B.8})$$

³Note that the logarithms in the bracket do not become large except for the extreme forward and backward region, which are anyhow not experimentally accessible at high-energy muon colliders.

respectively. We give here for completeness the explicit expression for the quantities $E_{s,\lambda}^\kappa$, $F_{s,\lambda}^\kappa$, $E_{\text{PR},\lambda}^\kappa$ and $F_{\text{PR},\lambda}^\kappa$:

$$E_{s,T}^\kappa = 3C_{\mu^\kappa}^{ew} + 2C_\Phi^{ew} + \frac{1}{2}b_{ZZ}^{ew} - \frac{3}{4s_w^2} \frac{m_t^2}{M_W^2} \quad (\text{B.9a})$$

$$E_{s,L}^\kappa = 3C_{\mu^\kappa}^{ew} + 4C_\Phi^{ew} - \frac{3}{2s_w^2} \frac{m_t^2}{M_W^2} \quad (\text{B.9b})$$

$$F_{s,T}^\kappa = \left(\frac{3}{4s_w^2} \frac{m_t^2}{M_W^2} + T_{ZZ} \right) \log \frac{m_t^2}{M_W^2} + \left(\frac{M_Z^2}{24s_w^2 M_W^2} - 2C_\Phi^{ew} \right) \log \frac{M_H^2}{M_W^2} \quad (\text{B.9c})$$

$$F_{s,L}^\kappa = \frac{3}{2s_w^2} \frac{m_t^2}{M_W^2} \log \frac{m_t^2}{M_W^2} + \left(\frac{M_Z^2}{8s_w^2 M_W^2} - 2C_\Phi^{ew} \right) \log \frac{M_H^2}{M_W^2} \quad (\text{B.9d})$$

$$E_{\text{PR},T}^\kappa = -b_{WW}^{ew} + \rho_{\mu^\kappa} \frac{s_w}{c_w} b_{AZ}^{ew} + 2C_\Phi^{ew} - \frac{1}{2}b_{ZZ}^{ew} - \frac{3}{4s_w^2} \frac{m_t^2}{M_W^2} \quad (\text{B.9e})$$

$$E_{\text{PR},L}^\kappa = -b_{WW}^{ew} + \rho_{\mu^\kappa} \frac{s_w}{c_w} b_{AZ}^{ew} \quad (\text{B.9f})$$

$$F_{\text{PR},T}^\kappa = \frac{5}{6} \left(\frac{1}{s_w^2} + \frac{\rho_{\mu^\kappa}}{c_w^2} - \frac{M_Z^2}{2s_w^2 M_W^2} \right) \log \frac{M_H^2}{M_W^2} - \left[\frac{9 + 6s_w^2 - 32s_w^4}{18s_w^2} \left(\frac{1}{s_w^2} + \frac{\rho_{\mu^\kappa}}{c_w^2} \right) + T_{ZZ} - \frac{3}{4s_w^2} \frac{m_t^2}{M_W^2} \right] \log \frac{m_t^2}{M_W^2} \quad (\text{B.9g})$$

$$F_{\text{PR},L}^\kappa = \left(\frac{1}{s_w^2} + \frac{\rho_{\mu^\kappa}}{c_w^2} \right) \left[\frac{5}{6} \log \frac{M_H^2}{M_W^2} - \frac{9 + 6s_w^2 - 32s_w^4}{18s_w^2} \log \frac{m_t^2}{M_W^2} \right] \quad (\text{B.9h})$$

The explicit values of the β -function coefficients b_{ZZ}^{ew} , b_{AZ}^{ew} and b_{WW}^{ew} and the numerical coefficient T_{ZZ} used here are (cf. [61]):

$$b_{ZZ}^{ew} = \frac{19 - 38s_w^2 - 22s_w^4}{6s_w^2 c_w^2} \quad b_{AZ}^{ew} = -\frac{19 + 22s_w^2}{6s_w c_w} \quad b_{WW}^{ew} = \frac{19}{6s_w^2} \quad (\text{B.10a})$$

$$T_{ZZ} = \frac{9 - 24s_w^2 + 32s_w^4}{36s_w^2 c_w^2} \quad . \quad (\text{B.10b})$$

The constants $E_{\text{PR},\lambda}^\kappa$ and $F_{\text{PR},\lambda}^\kappa$ depend on the parameter ρ_{μ^κ} which is defined by the EW quantum numbers of the muon as [46]

$$\rho_{\mu^\kappa} = \frac{Q_\mu - T_{\mu^\kappa}^3}{T_{\mu^\kappa}^3 - Q_\mu s_w^2} \quad . \quad (\text{B.11})$$

Summing the contributions from Eqs. (B.2), (B.5) and (B.8), the overall Sudakov factor as a function of the muon chirality κ and Z boson polarization λ can be formulated as

$$\Lambda_\lambda^\kappa = \Lambda_{l,\lambda}^\kappa + \Lambda_{\theta,\lambda}^\kappa + \Lambda_{s,\lambda}^\kappa + \Lambda_{\text{PR},\lambda}^\kappa \quad . \quad (\text{B.12})$$

This factor can now be used for an approximation of the relative NLO correction to the unpolarized process for which the photon radiation effects are subtracted, i. e. emulating the virtual EW effects in the high-energy limit. For the definition of this correction factor we apply two different approximations. The first one estimates

$$\Lambda_\lambda^\kappa \mathcal{M}_0^{\mu_\kappa^+ \mu_\kappa^- \rightarrow HZ_\lambda} \xrightarrow{s \gg M_W^2} \delta_{\lambda L} \Lambda_\lambda^\kappa \mathcal{M}_0^{\mu_\kappa^+ \mu_\kappa^- \rightarrow HZ_\lambda} \quad (\text{B.13})$$

since the Born amplitudes for transverse polarized Z bosons are suppressed by M_Z^2/s [47, 48].

For the second approximation, we assume amplitudes with the helicity configurations $(+, +)$ and $(-, -)$ of the muons to vanish due to the ultra-relativistic initial state momenta in the process. We thus arrive at a factor of the form

$$\Lambda_{\text{est}}^{\text{unpol}} = \frac{\sum_{\kappa} \Lambda_L^{\kappa} \left| \mathcal{M}_0^{\mu^+ \mu_{\kappa}^- \rightarrow HZ_L} \right|^2}{4 \left| \mathcal{M}_0^{\mu^+ \mu^- \rightarrow HZ_L} \right|^2} \quad (\text{B.14})$$

which approximates the non-integrated virtual corrections for unpolarized beams in the high-energy limit, when multiplied with unpolarized Born squared amplitudes $\left| \mathcal{M}_0^{\mu^+ \mu^- \rightarrow HZ_L} \right|^2$. Using the fact that the amplitudes depend on the muon chiralities only through the EW couplings, the angular dependency of squared Born amplitudes exclusive in the muon chiralities normalized to the unpolarized ones, drops out. From this, we find

$$\frac{\left| \mathcal{M}_0^{\mu_{\kappa}^+ \mu_{\kappa}^- \rightarrow HZ_L} \right|^2}{\left| \mathcal{M}_0^{\mu^+ \mu^- \rightarrow HZ_L} \right|^2} = \frac{\left(d\sigma_B^{\mu_{\kappa}^+ \mu_{\kappa}^- \rightarrow HZ_L} / d\Omega \right)}{\left(d\sigma_B^{\mu^+ \mu^- \rightarrow HZ_L} / d\Omega \right)} = \frac{\sigma_B^{\mu_{\kappa}^+ \mu_{\kappa}^- \rightarrow HZ_L}}{\sigma_B^{\mu^+ \mu^- \rightarrow HZ_L}} = \frac{\sigma_B^{\mu_{\kappa}^+ \mu_{\kappa}^- \rightarrow HZ}}{\sigma_B^{\mu^+ \mu^- \rightarrow HZ}} \quad . \quad (\text{B.15})$$

Hence, in our approach Eq. (B.14) can be rewritten as

$$\Lambda_{\text{est}}^{\text{unpol}} = \frac{1}{4} \frac{\sum_{\kappa} \Lambda_L^{\kappa} \sigma_B^{\mu_{\kappa}^+ \mu_{\kappa}^- \rightarrow HZ}}{\sigma_B^{\mu^+ \mu^- \rightarrow HZ}} \quad . \quad (\text{B.16})$$

For the evaluation of this approximative correction factor, integrated polarized and unpolarized Born cross sections σ_B obtained with the WHIZARD+RECOLA framework are used. The analytical Sudakov factors from Eqs. (B.12) and the factor of Eq. (B.16) for the (central) scattering angle $\theta_H = 90^\circ$ as well as $\Lambda_{\text{est},c}^{\text{unpol}}$, i. e. Eq. (B.16) with the angular-dependent terms $\Lambda_{\theta,L}^{\kappa}$ dropped, are depicted in Fig. 3 as a function of the center-of-mass energy in the main text. There, in Sec. 3.1, also the physics implications of the Sudakov factors and their comparison with the complete fixed-order NLO EW cross sections are discussed.

References

- [1] FCC collaboration, *FCC Physics Opportunities: Future Circular Collider Conceptual Design Report Volume 1*, *Eur. Phys. J. C* **79** (2019) 474.
- [2] FCC collaboration, *FCC-hh: The Hadron Collider: Future Circular Collider Conceptual Design Report Volume 3*, *Eur. Phys. J. ST* **228** (2019) 755.
- [3] H. Baer et al., *The International Linear Collider Technical Design Report - Volume 2: Physics*, **1306.6352**.
- [4] H. Abramowicz et al., *The International Linear Collider Technical Design Report - Volume 4: Detectors*, **1306.6329**.
- [5] CLIC, CLICDP collaboration, *Updated baseline for a staged Compact Linear Collider*, **1608.07537**.

- [6] M. Aicheler et al., *A Multi-TeV Linear Collider Based on CLIC Technology: CLIC Conceptual Design Report*, [CERN-2012-007](#).
- [7] J.P. Delahaye, M. Diemoz, K. Long, B. Mansoulié, N. Pastrone, L. Rivkin et al., *Muon Colliders*, [1901.06150](#).
- [8] N. Bartosik et al., *Detector and Physics Performance at a Muon Collider*, *JINST* **15** (2020) P05001 [[2001.04431](#)].
- [9] D. Schulte, J.-P. Delahaye, M. Diemoz, K. Long, B. Mansoulié, N. Pastrone et al., *Prospects on Muon Colliders*, *PoS ICHEP2020* (2021) 703.
- [10] K.R. Long, D. Lucchesi, M.A. Palmer, N. Pastrone, D. Schulte and V. Shiltsev, *Muon colliders to expand frontiers of particle physics*, [FERMILAB-PUB-21-040-AD](#).
- [11] C. Aime et al., *Muon Collider Physics Summary*, [2203.07256](#).
- [12] MUON COLLIDER collaboration, *The physics case of a 3 TeV muon collider stage*, [2203.07261](#).
- [13] CLIC collaboration, *The CLIC Potential for New Physics*, [1812.02093](#).
- [14] A. Costantini, F. De Lillo, F. Maltoni, L. Mantani, O. Mattelaer, R. Ruiz et al., *Vector boson fusion at multi-TeV muon colliders*, *JHEP* **09** (2020) 080 [[2005.10289](#)].
- [15] T. Han, D. Liu, I. Low and X. Wang, *Electroweak couplings of the Higgs boson at a multi-TeV muon collider*, *Phys. Rev. D* **103** (2021) 013002 [[2008.12204](#)].
- [16] M. Chiesa, F. Maltoni, L. Mantani, B. Mele, F. Piccinini and X. Zhao, *Measuring the quartic Higgs self-coupling at a multi-TeV muon collider*, *JHEP* **09** (2020) 098 [[2003.13628](#)].
- [17] R. Dermisek, K. Hermanek and N. McGinnis, *Di-Higgs and tri-Higgs boson signals of muon $g-2$ at a muon collider*, *Phys. Rev. D* **104** (2021) L091301 [[2108.10950](#)].
- [18] T. Han, W. Kilian, N. Kreher, Y. Ma, J. Reuter, T. Striegl et al., *Precision test of the muon-Higgs coupling at a high-energy muon collider*, *JHEP* **12** (2021) 162 [[2108.05362](#)].
- [19] W. Kilian, T. Ohl and J. Reuter, *WHIZARD: Simulating Multi-Particle Processes at LHC and ILC*, *Eur. Phys. J. C* **71** (2011) 1742 [[0708.4233](#)].
- [20] M. Moretti, T. Ohl and J. Reuter, *O'Mega: An Optimizing matrix element generator*, [hep-ph/0102195](#).
- [21] S. Braß, P. Bredt, W. Kilian, J. Reuter, V. Rothe and P. Stenemeier, *Automation of NLO SM processes in WHIZARD for hadron and lepton collisions, in preparation*, 2022.
- [22] S. Actis, A. Denner, L. Hofer, J.-N. Lang, A. Scharf and S. Uccirati, *RECOLA: REcursive Computation of One-Loop Amplitudes*, *Comput. Phys. Commun.* **214** (2017) 140 [[1605.01090](#)].
- [23] F. Buccioni, J.-N. Lang, J.M. Lindert, P. Maierhöfer, S. Pozzorini, H. Zhang et al., *OpenLoops 2*, *Eur. Phys. J. C* **79** (2019) 866 [[1907.13071](#)].
- [24] S. Frixione, Z. Kunszt and A. Signer, *Three jet cross-sections to next-to-leading order*, *Nucl. Phys. B* **467** (1996) 399 [[hep-ph/9512328](#)].
- [25] S. Frixione, *A General approach to jet cross-sections in QCD*, *Nucl. Phys. B* **507** (1997) 295 [[hep-ph/9706545](#)].
- [26] W. Kilian, T. Ohl, J. Reuter and C. Speckner, *QCD in the Color-Flow Representation*, *JHEP* **10** (2012) 022 [[1206.3700](#)].

- [27] B. Chokouf  Nejad, W. Kilian, J.M. Lindert, S. Pozzorini, J. Reuter and C. Weiss, *NLO QCD predictions for off-shell $t\bar{t}$ and $t\bar{t}H$ production and decay at a linear collider*, *JHEP* **12** (2016) 075 [[1609.03390](#)].
- [28] W. Kilian, J. Reuter and T. Robens, *NLO Event Generation for Chargino Production at the ILC*, *Eur. Phys. J. C* **48** (2006) 389 [[hep-ph/0607127](#)].
- [29] T. Robens, J. Kalinowski, K. Rolbiecki, W. Kilian and J. Reuter, *(N)LO Simulation of Chargino Production and Decay*, *Acta Phys. Polon. B* **39** (2008) 1705 [[0803.4161](#)].
- [30] T. Binoth, N. Greiner, A. Guffanti, J. Reuter, J.P. Guillet and T. Reiter, *Next-to-leading order QCD corrections to $pp \rightarrow b \text{ anti-}b b \text{ anti-}b + X$ at the LHC: the quark induced case*, *Phys. Lett. B* **685** (2010) 293 [[0910.4379](#)].
- [31] N. Greiner, A. Guffanti, T. Reiter and J. Reuter, *NLO QCD corrections to the production of two bottom-antibottom pairs at the LHC*, *Phys. Rev. Lett.* **107** (2011) 102002 [[1105.3624](#)].
- [32] F. Bach, B.C. Nejad, A. Hoang, W. Kilian, J. Reuter, M. Stahlhofen et al., *Fully-differential Top-Pair Production at a Lepton Collider: From Threshold to Continuum*, *JHEP* **03** (2018) 184 [[1712.02220](#)].
- [33] S. Dittmaier and C. Schwan, *Non-factorizable photonic corrections to resonant production and decay of many unstable particles*, *Eur. Phys. J. C* **76** (2016) 144 [[1511.01698](#)].
- [34] A. Denner, S. Dittmaier, M. Roth and D. Wackeroth, *Electroweak radiative corrections to $e^+e^- \rightarrow W^+W^- \rightarrow 4$ fermions in double pole approximation: The RACOONWW approach*, *Nucl. Phys. B* **587** (2000) 67 [[hep-ph/0006307](#)].
- [35] T. Ohl, *Vegas revisited: Adaptive Monte Carlo integration beyond factorization*, *Comput. Phys. Commun.* **120** (1999) 13 [[hep-ph/9806432](#)].
- [36] S. Brass, W. Kilian and J. Reuter, *Parallel Adaptive Monte Carlo Integration with the Event Generator WHIZARD*, *Eur. Phys. J. C* **79** (2019) 344 [[1811.09711](#)].
- [37] R.R. Sadykov, A.B. Arbuzov, S.G. Bondarenko, Y.V. Dydyshka, L.V. Kalinovskaya, I.I. Novikov et al., *MCSANee generator with one-loop electroweak corrections for processes with polarized e^+e^- beams*, *J. Phys. Conf. Ser.* **1525** (2020) 012012.
- [38] P. Nogueira and J.C. Romao, *Initial-final state interference in $e^+e^- \rightarrow H \mu^+ \mu^-$* , *Z. Phys. C* **60** (1993) 757.
- [39] B.A. Kniehl, *Higgs phenomenology at one loop in the standard model*, *Phys. Rept.* **240** (1994) 211.
- [40] G. Belanger, F. Boudjema, J. Fujimoto, T. Ishikawa, T. Kaneko, K. Kato et al., *Full one loop electroweak radiative corrections to single Higgs production in e^+e^-* , *Phys. Lett. B* **559** (2003) 252 [[hep-ph/0212261](#)].
- [41] Q. Song and A. Freitas, *On the evaluation of two-loop electroweak box diagrams for $e^+e^- \rightarrow HZ$ production*, *JHEP* **04** (2021) 179 [[2101.00308](#)].
- [42] J.H. Kuhn, A.A. Penin and V.A. Smirnov, *Summing up subleading Sudakov logarithms*, *Eur. Phys. J. C* **17** (2000) 97 [[hep-ph/9912503](#)].
- [43] A. Denner and S. Pozzorini, *One loop leading logarithms in electroweak radiative corrections. 1. Results*, *Eur. Phys. J. C* **18** (2001) 461 [[hep-ph/0010201](#)].
- [44] A. Denner and S. Pozzorini, *One loop leading logarithms in electroweak radiative corrections. 2. Factorization of collinear singularities*, *Eur. Phys. J. C* **21** (2001) 63 [[hep-ph/0104127](#)].

- [45] G. Bell, J.H. Kuhn and J. Rittinger, *Electroweak Sudakov Logarithms and Real Gauge-Boson Radiation in the TeV Region*, *Eur. Phys. J. C* **70** (2010) 659 [[1004.4117](#)].
- [46] F. Granata, J.M. Lindert, C. Oleari and S. Pozzorini, *NLO QCD+EW predictions for HV and $HV + \text{jet}$ production including parton-shower effects*, *JHEP* **09** (2017) 012 [[1706.03522](#)].
- [47] M.S. Chanowitz and M.K. Gaillard, *The TeV Physics of Strongly Interacting W 's and Z 's*, *Nucl. Phys. B* **261** (1985) 379.
- [48] M. Bohm, A. Denner and H. Joos, *Gauge theories of the strong and electroweak interaction*, Teubner Verlag; 3rd rev. ed. 2001 Edition (2001), [10.1007/978-3-322-80160-9](#).
- [49] A. Denner and T. Sack, *ELECTROWEAK RADIATIVE CORRECTIONS TO $e^+ e^- \rightarrow Z0$* , *Nucl. Phys. B* **306** (1988) 221.
- [50] M. Cacciari, A. Deandrea, G. Montagna and O. Nicrosini, *QED structure functions: A Systematic approach*, *EPL* **17** (1992) 123.
- [51] M. Skrzypek and S. Jadach, *Exact and approximate solutions for the electron nonsinglet structure function in QED*, *Z. Phys. C* **49** (1991) 577.
- [52] M. Skrzypek, *Leading logarithmic calculations of QED corrections at LEP*, *Acta Phys. Polon. B* **23** (1992) 135.
- [53] S. Frixione, *Initial conditions for electron and photon structure and fragmentation functions*, *JHEP* **11** (2019) 158 [[1909.03886](#)].
- [54] V. Bertone, M. Cacciari, S. Frixione and G. Stagnitto, *The partonic structure of the electron at the next-to-leading logarithmic accuracy in QED*, *JHEP* **03** (2020) 135 [[1911.12040](#)].
- [55] V. Bertone, M. Cacciari, S. Frixione, G. Stagnitto, M. Zaro and X. Zhao, *Improving methods and predictions at high-energy e^+e^- colliders within collinear factorisation*, [2207.03265](#).
- [56] T. Han, Y. Ma and K. Xie, *High Energy Leptonic Collisions and Electroweak Parton Distribution Functions*, [2007.14300](#).
- [57] W. Beenakker, A. Denner, S. Dittmaier, R. Mertig and T. Sack, *High-energy approximation for on-shell W pair production*, *Nucl. Phys. B* **410** (1993) 245.
- [58] W. Beenakker and A. Denner, *Standard model predictions for W pair production in electron - positron collisions*, *Int. J. Mod. Phys. A* **9** (1994) 4837.
- [59] Berggren, M., *private communication*, 2022.
- [60] P. Bredt, W. Kilian, K. Mękała, J. Reuter and A. Żarnecki, *Precision study of multi-boson processes at a muon collider, in preparation*, 2022.
- [61] S. Pozzorini, *Electroweak radiative corrections at high-energies*, other thesis, University of Zürich, 2001, [[hep-ph/0201077](#)].